HHS Public Access

Author manuscript

J Vis Exp. Author manuscript; available in PMC 2022 December 09.

Single-Particle Cryo-EM Data Collection with Stage Tilt using Leginon

Sriram Aiyer[1], **Timothy S. Strutzenberg**[1], **Marianne E. Bowman**[2], **Joseph P. Noel**[2,3], **Dmitry Lyumkis**[1,4,5]

[1]Laboratory of Genetics, The Salk Institute for Biological Studies

[2]Jack H. Skirball Center for Chemical Biology and Proteomics, The Salk Institute for Biological Studies

[3]Department of Chemistry and Biochemistry, University of California San Diego

[4]Graduate School of Biological Sciences, Section of Molecular Biology, University of California San Diego

[5]Department of Integrative Structural and Computational Biology, The Scripps Research Institute

Abstract

Single-particle analysis (SPA) by cryo-electron microscopy (cryo-EM) is now a mainstream technique for high-resolution structural biology. Structure determination by SPA relies upon obtaining multiple distinct views of a macromolecular object vitrified within a thin layer of ice. Ideally, a collection of uniformly distributed random projection orientations would amount to all possible views of the object, giving rise to reconstructions characterized by isotropic directional resolution. However, in reality, many samples suffer from preferentially oriented particles adhering to the air-water interface. This leads to non-uniform angular orientation distributions in the dataset and inhomogeneous Fourier-space sampling in the reconstruction, translating into maps characterized by anisotropic resolution. Tilting the specimen stage provides a generalizable solution to overcoming resolution anisotropy by virtue of improving the uniformity of orientation distributions, and thus the isotropy of Fourier space sampling. The present protocol describes a tilted-stage automated data collection strategy using Leginon, a software for automated image acquisition. The procedure is simple to implement, does not require any additional equipment or software, and is compatible with most standard transmission electron microscopes (TEMs) used for imaging biological macromolecules.

Introduction

The advent of direct electron detectors over the past decade[1, 2, 3] has spurred an exponential increase in the number of high-resolution structures of macromolecules and macromolecular

Corresponding Author: Dmitry Lyumkis dlyumkis@salk.edu.

A complete version of this article that includes the video component is available at http://dx.doi.org/10.3791/64136.

Disclosures

The authors have nothing to disclose.

assemblies solved using single-particle cryo-EM[4, 5, 6]. Almost all purified macromolecular species are expected to be amenable to structure determination using cryo-EM, except for the smallest proteins ~10 kDa in size or below[7]. The amount of starting material needed for grid preparation and structure determination is at least an order of magnitude less than other structure determination techniques, such as nuclear magnetic resonance spectroscopy and X-ray crystallography[4, 5, 6].

However, a principal challenge for structure determination by cryo-EM involves suitable grid preparation for imaging. An extensive study evaluating diverse samples using different vitrification strategies and grids suggested that most approaches for vitrifying samples on cryo-EM grids lead to preferential adherence of macromolecules to the air-water interface[8]. Such adherence can potentially cause four suboptimal outcomes: (1) the macromolecular sample completely denatures, in which case no successful data collection and processing is possible; (2) the sample partially denatures, in which case it may be possible to obtain structural insights from regions of the macromolecule that are not damaged; (3) the sample retains native structure, but only one set of particle orientations relative to the direction of the electron beam are represented in the images; (4) the sample retains native structure, and some but not all possible particle orientations relative to the direction of the electron beam are represented in the images. For cases (3) and (4), tilted data collection will help with minimizing directional resolution anisotropy affecting the reconstructed cryo-EM map and provides a generalizable solution for a wide variety of samples[9]. Technically, tilting can also benefit case (2), since the denaturation presumably occurs at the air-water interface and similarly limits the number of distinct orientations represented within the data. The extent of orientation bias in the dataset can potentially be altered by experimenting with solution additives, but a lack of broad applicability hampers these trial-and-error approaches. Tilting the specimen stage at a single optimized tilt angle is sufficient to improve the distribution of orientations by virtue of altering the geometry of the imaging experiment[9] (Figure 1). Due to the geometric configuration of the preferentially-oriented sample with respect to the electron beam, for each cluster of preferential orientations, tilting the grid generates a cone of illumination angles with respect to the cluster centroid. Hence, this spreads out the views and consequently improves Fourier space sampling and the isotropy of directional resolution.

There are, in practice, some detriments to tilting the stage. Tilting the specimen stage introduces a focus gradient across the field of view, which may affect the accuracy of contrast transfer function (CTF) estimations. Tilted data collection may also lead to increased beam-induced particle movement caused by increased charging effects when imaging tilted specimens. Grid tilting also leads to an increase in apparent ice thickness, which in turn leads to noisier micrographs and may ultimately impact the resolution of reconstructions[5, 9, 10]. It may be possible to overcome these issues by applying advanced computational data-processing schemes that are briefly described in the protocol and discussion sections. Lastly, tilting can lead to increased particle overlap, hindering the subsequent image processing pipeline. Although this can be mitigated to some extent by optimizing on-grid particle concentration, it is nonetheless an important consideration. Here, a simple-to-implement protocol is described for tilted data collection using the Leginon software suite (an automated image acquisition software), available open access

and compatible with a broad range of microscopes[11, 12, 13, 14]. The method requires at least version 3.0 or higher, with versions 3.3 onward containing dedicated improvements to enable tilted data collection. No additional software or equipment is necessary for this protocol. Extensive instructions on computational infrastructure and installation guides are provided elsewhere[15].

Protocol

1. Sample preparation

1. Use grids containing gold foil and gold grid support[16] (see Table of Materials) because tilted data collection can accentuate beam-induced motion[17].

   NOTE: For the present study, samples on grids were vitrified using the manual plunging and blotting technique[18] in a humidified (greater than 80%) cold room (~4 °C).

2. Avoid using grids containing copper support and carbon foil or a continuous layer of amorphous carbon unless absolutely necessary, as these grids may lead to greater beam-induced motion[16] when the specimen stage is tilted.

   NOTE: Alternative support layers, such as graphene/graphene oxide, appear to reduce beam-induced movement compared to amorphous carbon[19, 20].

3. Pre-screen grids and identify regions characterized by acceptable ice thickness and particle distribution. Grids containing too tightly packed particles will lead to particle overlap during tilted data collection, which may affect downstream data-processing steps.

   NOTE: These steps are subjective since identifying good areas of ice is performed by visually inspecting defocused images for regions where particle contrast is clear. This may not be feasible for all samples since some samples will not distribute efficiently in areas of thin ice, leading to challenges during data collection (described in the Discussion section).

4. Vitrify the grids containing your protein sample. Here, for demonstration purposes, we use DNA Protection during Starvation (DPS) protein (see Table of Materials) at a range from 0.1–0.5 mg/mL with gold foil and gold support grids.

   NOTE: The protein was purified as described previously, except no TEV protease cleavage was performed[21]. The protein concentration range for a sample of interest will have to be optimized individually, since it is hard to gauge an ideal range that is universally applicable and will almost certainly vary between different samples.

2. Setting up tilted data collection

1. Align the microscope to ensure parallel illumination of the specimen and minimize coma aberrations[22].

NOTE: The microscope must be well aligned for standard SPA data collection without stage tilt. No special alignments are necessary for tilted data collection, but a good alignment will ensure that targeting and imaging proceed smoothly. A general scheme comparing tilted and untilted data collection is provided in Figure 2.

2. Record a grid atlas without stage tilt to identify squares suitable for data collection or manually inspect squares at the magnification used in **Square Acquisition Node**. Look for squares where the foil is intact, does not look dehydrated, and has ideal ice thickness.

   NOTE: **Square Acquisition Node** is the low-magnification node used for multi-scale imaging in Leginon.

   1. For typical untilted automated data collection, record a grid atlas, which provides an overview of the overall grid quality and an initial indication of suitable areas for data collection.
   2. Subsequently, select suitable squares through the atlas and submit them to the queue. Then, either through manual selection of holes or through the automated EM hole finder, queue and submit the hole targets.
   3. Finally, use the automated EM hole finder for submitting high magnification exposure targets.

      NOTE: For tilted data collection, squares may need to be queued manually for consistent results, especially if the optimal tilt angle has not been pre-determined and is likely to be adjusted during data collection. The grid atlas could also be recorded using a pre-defined stage tilt if the tilt angle used for data collection had previously been established.

3. Move the specimen stage to a square of interest.

4. Determine the eucentric height for the stage position using α-wobbler at ± 15° stage tilt. Adjust the Z-height to bring the stage to eucentric height using the keypad panel for the microscope. Ensure the image shift is minimal during the α-wobble routine.

   NOTE: If the eucentric height is not properly identified, a large image shift will be observed upon tilting the stage at the square magnification. This can also happen if there are local deformations on the grid, for example, if the grid is broken or severely bent in the vicinity of the imaged area. Although it is best to avoid such regions for data collection, it is imperative to accurately estimate eucentric height if these represent one of the few promising regions for data collection. Figure 3 shows how targeting without properly identifying eucentric height can cause large image shifts in the square magnification.

5. Find a more accurate Z-height, use the **Focuser node**, and press **Simulate**.

1. Typically, estimate the Z-height in the **Focuser node** at the magnification used in **Square Acquisition Node**.

   NOTE: The **Focuser node** focus sequence can also include a fine Z focus estimation at the **Hole Acquisition node** (a tool in Leginon software) magnification during data collection.

2. Adjust the settings for the **Focuser node** and enable/disable the fine Z focus option during the initial queuing of squares.

   NOTE: It is important to ensure that eucentric height is accurately identified when automated data collection begins, which may require re-enabling fine Z focus (step 2.10).

6. Tilt the specimen stage to the desired tilt angle for data collection at the true eucentric height, and re-center the stage if necessary. 0°, 30°, and 60° tilt angles were used for this study. Press **Simulate** in the **Square Acquisition node** to begin queuing targets for **Hole Acquisition node** exposures.

   NOTE: As indicated in step 2.2.1, the grid atlas can be recorded using a pre-defined stage tilt, which would obviate the need to tilt the stage again at this step. This works well and speeds up the process if the tilt angle used for data collection is pre-defined. The current protocol is written with new specimens in mind, wherein the user may wish to test different tilt angles for data collection.

7. Select a **Z focus** target and regions with holes suitable for high magnification exposures.

8. Press **Submit targets to queue** for imaging. Do not press Submit Queued Targets until finished queuing up all squares.

9. Bring the specimen stage back to its untilted state. Move to the next square and repeat steps 2.3–2.8 until an adequate number of hole exposures have been queued.

10. Go to the **Hole Targeting Node** and press **Submit Queued Targets** once all squares are queued.

    NOTE: If fine Z focus was disabled previously to save time (step 2.5), it needs to be re-enabled before submitting the queue.

11. Manually inspect targets selected by the high magnification **Exposure Acquisition node** to test if the automated EM hole finder can accurately identify suitable regions for image acquisition when the specimen stage is tilted.

    1. During this procedure, select ‘Allow for user verification of selected targets’ in **Exposure Acquisition node** settings. Once the user is satisfied with targeting accuracy, deselect this option for automated data collection.

       NOTE: Targets in high magnification **Exposure Acquisition node** are typically imaged using a beam-tilt image shift strategy, which works

equally well for both tilted and untilted data collection[23, 24, 25, 26]. For accurate CTF estimation in downstream data processing steps, the lenscoma aberration calibration must be performed for the beam-tilt image shift data collection strategy.

3. Data Processing

1. Initiate on-the-fly data processing[10, 27, 28, 29] with motion-correction of recordedmovies, CTF estimation, particle selection, and generation of initial reconstructions during data collection.

   NOTE: For the present study, cryoSPARC Live[10] (see Table of Materials) has been utilized for pre-processing. On-the-fly data processing provides an initial cryo-EM reconstruction and an approximation for the angular distribution, which can inform the user about the extent of resolution anisotropy. These can, in turn, be used to guide the user as to whether or not the tilt angle used for data collection is sufficiently high.

2. Visualize the reconstructed map and plot the Euler angle distribution to gauge the extent of preferred particle orientations.

   NOTE: The Euler angle distributions can be converted directly into Fourier space sampling distributions to determine the potential extent of resolution anisotropy. A graphical user interface (GUI) has been developed to assist the user in evaluating the quality of an Euler angle distribution and determining an optimal tilt angle[30, 31]. The tool can be obtained from the Github repository, https://github.com/LyumkisLab/SamplingGui.

3. If necessary, adjust the stage tilt angle at which data is collected to overcome the effects of preferential orientation. The angle can be increased if the preferential orientation remains a problem, as evidenced by the map and Euler distribution in 3.2. Alternatively, the user may wish to split the data collection into groups and record using several different tilt angles, such as 20°, 30°, and 40°.

   NOTE: Although most TEMs must have the capability of tilting the stage to 70°, common specimen stage tilts (that we have used) range from 20°−40°.

Representative Results

DPS at 0.3 mg/mL was used to demonstrate imaging at 0°, 30°, and 60° tilts. Data from different tilt angles were collected on the same grid at different grid regions. CTF resolution fits for higher angle tilts tend to be poorer, as was the case when comparing the three datasets in this study. Figure 4 demonstrates comparative representative images and 2D classification averages. Although the protein concentration is unchanged across the different tilt angles, a higher tilt angle makes the imaged area appear more crowded in terms of particle concentration. This can be problematic for data processing because particle overlap can complicate 3D reconstructions and angular refinements. Iterative 2D classification routinely produced a clean stack of particles with the 0° and 30° tilted datasets, whereas the 60° dataset required careful cleaning of the particle stacks to ensure that class averages show

minimal overlap for adjacent particles. The class average from Figure 4C in the red box represents an example of particle overlap. Although re-centering during classification can result in the signal from neighboring particles getting averaged, substantial particle overlap can compromise the accuracy of particle alignment parameters, yielding reconstructions characterized by lower resolution. The best solution to avoid particle overlap is to pre-screen grids with optimal ice thickness and particle distribution. A comprehensive quantitative overview of the metrics to evaluate improvements from tilted data collection is described elsewhere[32].

Discussion

Preferred particle orientation caused by specimen adherence to the air-water interface is one of the last major bottlenecks to routine high-resolution structure determination using cryo-EM SPA[4, 5, 6]. The data collection scheme presented here provides an easy-to-implement strategy for improving the orientation distribution of particles within a dataset. We note that the protocol requires no additional equipment or software and does not affect the data collection speed. The following considerations are important during data acquisition for tilted specimens.

Firstly, the imaged square must be at eucentric height for optimal targeting. Eucentric height is adjusted by recording tilt-pair images at small stage tilt angles (usually 0.5°−2°) and identifying focus based on a pre-defined relationship between image shift and defocus. If the targeted square requires a large adjustment in eucentric height, this will result in a significant image shift of the square image, such that when the stage is tilted again, the field of view may be blocked by the objective aperture.

Secondly, the normally circular hole becomes increasingly oblong with higher tilts at medium magnification (**Hole Acquisition Node** magnification). In the absence of accurate image-shift calibrations, it is possible that part of the foil may be imaged along with particles embedded in vitreous ice for a given exposure magnification. Therefore, ideally, the image-shift calibrations have to be accurate. An alternative is to increase the magnification such that the imaged area relative to hole size decreases. At higher magnification, errors in beam tilt-induced image-shift would have a smaller effect on a user's ability to navigate to an area of vitreous ice. However, this comes at the expense of diminishing the number of particles in the resulting micrographs, proportional to an increase in magnification.

Thirdly, autofocus has a greater chance of failing for tilted data collection due to increased beam-induced motion and increased specimen thickness. Thus, achieving accurate focus can, occasionally, present some challenges for tilted data collection, especially if the focus target is the gold foil in the center of four holes, which is standard practice for untilted data collection. In cases of frequent focus estimation failures, an alternative is to set the edge of a hole as the focus target. This must provide a sufficient signal for accurate phase correlation between beam tilt-induced image pairs and subsequent focus adjustment. In our experience, focusing on the edge of a hole rarely results in autofocus failure.

And lastly, when high-magnification images are selected far from the grid center, the difference in focus between targeted images on opposite sides of the tilt axis may be significant. The magnitude of this difference is dependent on the tilt angle and the distance from the point of focus. For example, at a tilt angle of 30°, two targets that are 6 μm apart on the surface of the grid and selected exactly perpendicular to the tilt axis will have a 3 μm difference in defocus between them (the relationship is: delta defocus = sin (tilt angle) * (distance from tilt axis)). Targets selected along the tilt axis will have the same defocus, whereas others will fall somewhere between. If the tilt axis is defined in Leginon during calibration, the software automatically compensates for the change in defocus. However, users must be aware that the possibility of having larger focus gradients during high-magnification imaging nonetheless exists. Large focus gradients should minimally affect the final reconstruction[33], but it may be necessary to use larger box sizes during data processing to prevent aliasing effects. Under these circumstances, using a narrower defocus range during data acquisition may be warranted, and randomization of defocus comes naturally from tilting the stage. Per-particle defocus adjustments during data processing can improve resolutions of final reconstructions. However, since accurate modeling of CTF fits may be challenging for high stage-tilt angles, care must be taken to monitor the quality of the data, and the CTF fits during exposure curation. Generally, sub-optimal ice thickness results in poorer accuracy in modeling CTF estimation fits. Therefore, care must be taken to image in areas where the ice is thin, assuming that the particle distribution is sufficiently good in these areas.

An improved and more uniform orientation distribution leads to a corresponding improvement in the directional resolution of the reconstructed cryo-EM maps. In addition, a more uniform orientation distribution improves the sampling compensation factor, which directly relates to global resolution[30, 31]. Thus, collectively improving the orientation distribution should improve the accuracy of atomic modeling and refinement[9, 30, 31]. This would, in principle, provide a strong case for routine implementation of tilted data collection. However, there are several caveats the user must be aware of. First, the increased focus gradient and ice thickness can impact overall global resolution, presumably due to a combination of increased background noise and increased beam-induced motion, combined with other indirect issues that arise as a result[17]. This effect is expected to be more pronounced in cases where the ice is inherently thicker. However, since most samples suffer from some amount of preferred orientation, which may in turn lead to sampling non-uniformity, tilted data collection may be generally beneficial as long as the detrimental effects are minimized or mitigated. Second, it may be necessary to tilt the stage as high as 60° for some samples characterized by severe preferential orientation. Anecdotal unpublished evidence from our work and colleagues' reports suggests that even ~40° tilts are insufficient to overcome resolution anisotropy for some specimens. Efforts toward identifying an optimal tilt angle for a set of distributions are underway, based on the ideas laid out in Baldwin et al.[31]. Lastly, one should note that, in principle, a reconstruction from a sample characterized by a perfectly pathological single preferred orientation would still have a 30° missing cone even when the data is collected at a 60° tilt angle. In simulated experiments, a 30° missing cone is unlikely to affect experimental interpretations greatly. A 60° tilt is probably sufficient for even the most pathologically preferentially oriented

specimens. However, in cases where the stage may have to be tilted by as much as 60°, the concentration of particles in the field of view needs to be carefully optimized, since particle overlap will complicate data processing. It is not possible to tilt to more than 60° (or 70° on select microscope stages) on standard TEMs, due to limitations of the sample stage design. In such cases, additional optimization with additives and sample biochemistry may be required.

Supplementary Material

Refer to Web version on PubMed Central for supplementary material.

Acknowledgments

We thank Bill Anderson, Charles Bowman, and Jean-Christophe Ducom (TSRI) for help with microscopy, Leginon installations, and data transfer infrastructure. We also thank Gordon Louie (Salk Institute) and Yong Zi Tan (National University of Singapore) for the critical reading of the manuscript. We thank Chris Russo (MRC Laboratory of Molecular Biology, Cambridge) for providing us with the plasmid for expression of DPS. This work was supported by grants from the US National Institutes of Health (U54AI150472 and R01AI136680 to DL), the National Science Foundation (NSF MCB-2048095 to DL), the Hearst Foundations (to DL), and Arthur and Julie Woodrow Chair (to J. P. N.).

References

1. Campbell MG et al. Movies of ice-embedded particles enhance resolution in electron cryo-microscopy. Structure 20 (11), 1823–1828 (2012). [PubMed: 23022349]
2. Bai XC, Fernandez IS, McMullan G, Scheres SH Ribosome structures to near-atomic resolution from thirty thousand cryo-EM particles. Elife 2, e00461 (2013). [PubMed: 23427024]
3. Li X et al. Electron counting and beam-induced motion correction enable near-atomic-resolution single-particle cryo-EM. Nature Methods 10 (6), 584–590 (2013). [PubMed: 23644547]
4. Chua EYD et al. Better, faster, cheaper: recent advances in cryo-electron microscopy. Annual Review of Biochemistry 10.1146/annurev-biochem-032620-110705, (2022).
5. Lyumkis D Challenges and opportunities in cryo-EM single-particle analysis. Journal of Biological Chemistry 294 (13), 5181–5197 (2019). [PubMed: 30804214]
6. Wu M, Lander GC Present and emerging methodologies in Cryo-EM single-particle analysis. Biophysical Journal 119 (7), 1281–1289 (2020). [PubMed: 32919493]
7. Henderson R The potential and limitations of neutrons, electrons and X-rays for atomic resolution microscopy of unstained biological molecules. Quarterly Reviews of Biophysics 28 (2), 171–193 (1995). [PubMed: 7568675]
8. Noble AJ et al. Routine single particle CryoEM sample and grid characterization by tomography. Elife 7, e34257 (2018). [PubMed: 29809143]
9. Tan YZ et al. Addressing preferred specimen orientation in single-particle cryo-EM through tilting. Nature Methods 14 (8), 793–796 (2017). [PubMed: 28671674]
10. Punjani A, Rubinstein JL, Fleet DJ, Brubaker MA cryoSPARC: algorithms for rapid unsupervised cryo-EM structure determination. Nature Methods 14 (3), 290–296 (2017). [PubMed: 28165473]
11. Potter CS et al. Leginon: a system for fully automated acquisition of 1000 electron micrographs a day. Ultramicroscopy 77 (3–4), 153–161 (1999). [PubMed: 10406132]
12. Suloway C et al. Automated molecular microscopy: The new Leginon system. Journal of Structural Biology 151 (1), 41–60 (2005). [PubMed: 15890530]
13. Cheng A et al. Leginon: New features and applications. Protein Science 30 (1), 136–150 (2021). [PubMed: 33030237]
14. Carragher B et al. Leginon: An automated system for acquisition of images from vitreous ice specimens. Journal of Structural Biology 132 (1), 33–45 (2000). [PubMed: 11121305]
15. Leginon https://emg.nysbc.org/redmine/projects/leginon/wiki/Leginon_Homepage. (2022).

16. Russo CJ, Passmore LA Electron microscopy: Ultrastable gold substrates for electron cryomicroscopy. Science 346 (6215), 1377–1380 (2014). [PubMed: 25504723]
17. Russo CJ, Henderson R Charge accumulation in electron cryomicroscopy. Ultramicroscopy 187, 43–49 (2018). [PubMed: 29413411]
18. Nguyen HPM, McGuire KL, Cook BD, Herzik MA Jr. Manual blot-and-plunge freezing of biological specimens for single-particle cryogenic electron microscopy. Journal of Visualized Experiments 180, e62765 (2022).
19. Patel A, Toso D, Litvak A, Nogales E Efficient graphene oxide coating improves cryo-EM sample preparation and data collection from tilted grids. bioRxiv 10.1101/2021.03.08.434344 2021.2003.2008.434344 (2021).
20. Naydenova K, Peet Mathew J, Russo Christopher J Multifunctional graphene supports for electron cryomicroscopy. Proceedings of the National Academy of Sciences 116 (24), 11718–11724 (2019).
21. Naydenova K et al. CryoEM at 100 keV: a demonstration and prospects. IUCrJ 6 (6), 1086–1098 (2019).
22. Herzik MA in cryoEM: Methods and Protocols 10.1007/978-1-0716-0966-8_6 eds (Gonen Tamir & Nannenga Brent L.) 125–144 Springer US, (2021).
23. Cash JN, Kearns S, Li Y, Cianfrocco MA High-resolution cryo-EM using beam-image shift at 200 keV. IUCrJ 7 (6), 1179–1187 (2020).
24. Peck JV, Fay JF, Strauss JD High-speed high-resolution data collection on a 200 keV cryo-TEM. IUCrJ 9 (2), 243–252 (2022).
25. Bouvette J et al. Beam image-shift accelerated data acquisition for near-atomic resolution single-particle cryo-electron tomography. Nature Communications 12 (1), 1957 (2021).
26. Cheng A et al. High resolution single particle cryo-electron microscopy using beam-image shift. Journal of Structural Biology 204 (2), 270–275 (2018). [PubMed: 30055234]
27. Tegunov D, Cramer P Real-time cryo-electron microscopy data preprocessing with Warp. Nature Methods 16 (11), 1146–1152 (2019). [PubMed: 31591575]
28. Structura Biotechnology Inc <https://cryosparc.com/live> (2022).
29. DiIorio MC, Kulczyk AW A robust single-particle cryo-electron microscopy (cryo-EM) processing workflow with cryoSPARC, RELION, and Scipion. Journal of Visualized Experiments 179, e63387 (2022).
30. Baldwin PR, Lyumkis D Non-uniformity of projection distributions attenuates resolution in Cryo-EM. Progress in Biophysics and Molecular Biology 150, 160–183 (2020). [PubMed: 31525386]
31. Baldwin PR, Lyumkis D Tools for visualizing and analyzing Fourier space sampling in Cryo-EM. Progress in Biophysics and Molecular Biology 160, 53–65 (2021). [PubMed: 32645314]
32. Aiyer S, Zhang C, Baldwin PR, Lyumkis D in cryoEM: Methods and Protocols 10.1007/978-1-0716-0966-8_8 eds (Gonen Tamir & Nannenga Brent L.) 161–187 Springer US, (2021).
33. Glaeser RM et al. Defocus-dependent Thon-ring fading. Ultramicroscopy 222, 113213 (2021). [PubMed: 33524638]

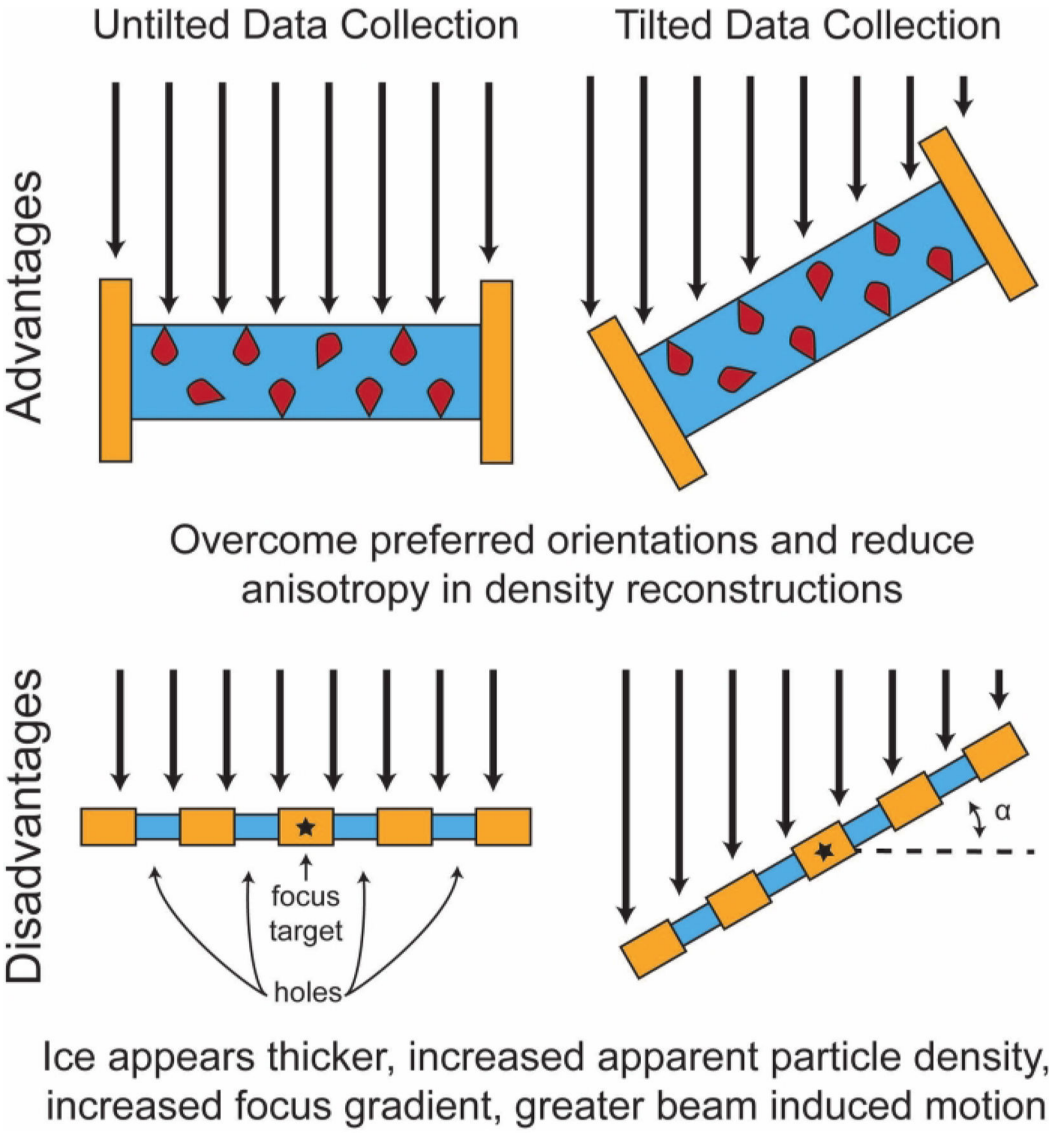

Figure 1: Overview of advantages and challenges with tilted data collection.

The top panel shows a close-up view of a grid hole. Grid bars are in gold, vitreous ice blue, and macromolecular particles red. Arrows indicate the direction of the electron beam. The bottom panel represents a collection of holes with the same coloring scheme as in the top panel. The black star represents the fine focus target prior to exposure image acquisition at high magnification. The tilt angle is indicated as 'α'.

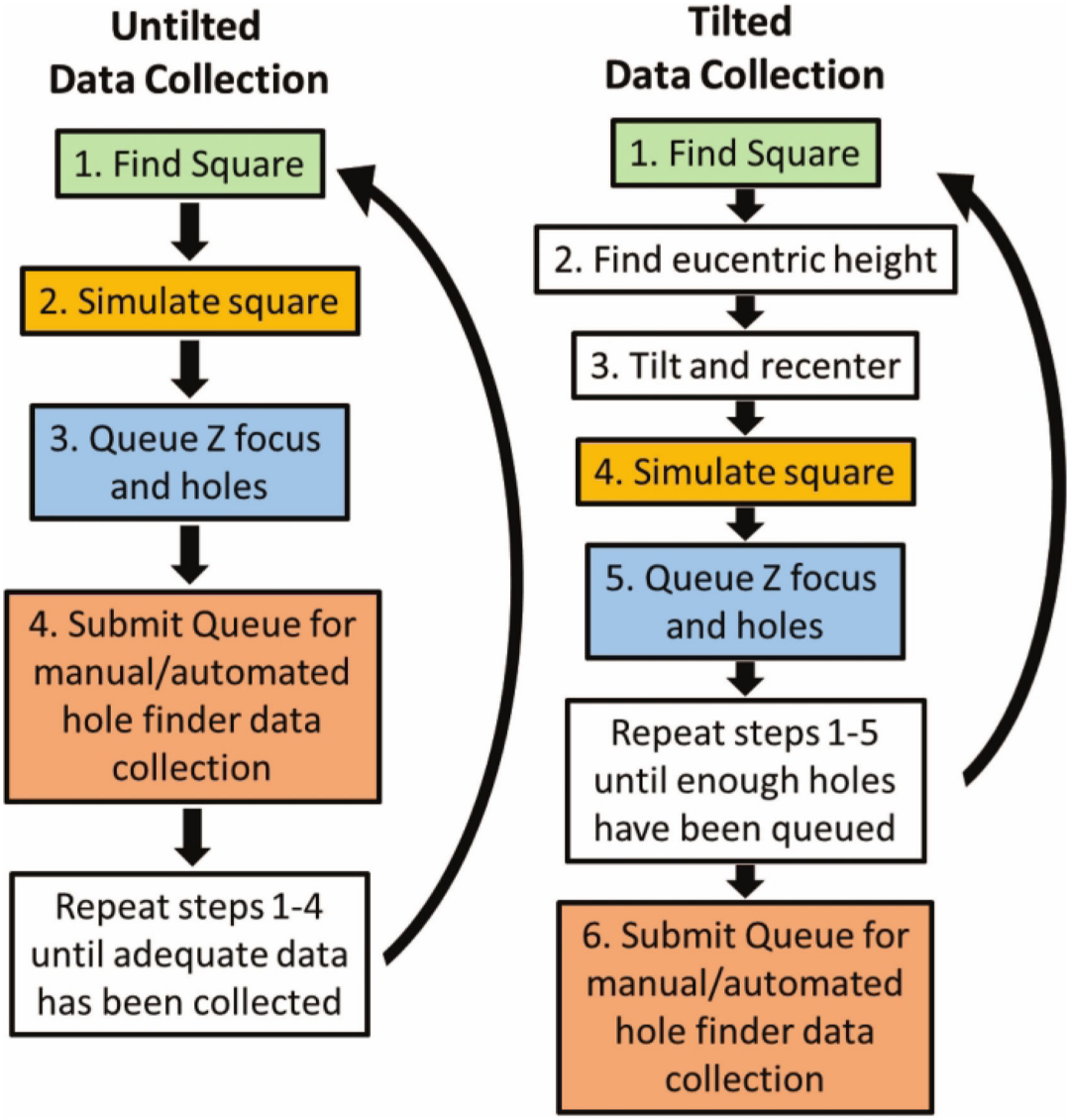

Figure 2: Workflow diagram comparing untilted and tilted data collection strategy.

Stepwise comparison of untilted and tilted data collection shows the additional step of manually estimating the eucentric height and re-centering for each tilted square (2 and 3 for tilted data collection). The rest of the workflow is similar between the two strategies. These include selecting a suitable square for imaging (1 for tilted and untilted data collection), initiating a queueing scheme by choosing a square for imaging (referred to as simulate; 2 and 4 for untilted and tilted data collection, respectively), providing a eucentric height focus target and queue hole magnification acquisition targets (3 and 5 for untilted and tilted data collection, respectively). and finally submitting the queue of selected high magnification exposure targets (4 and 6 for untilted and tilted data collection, respectively).

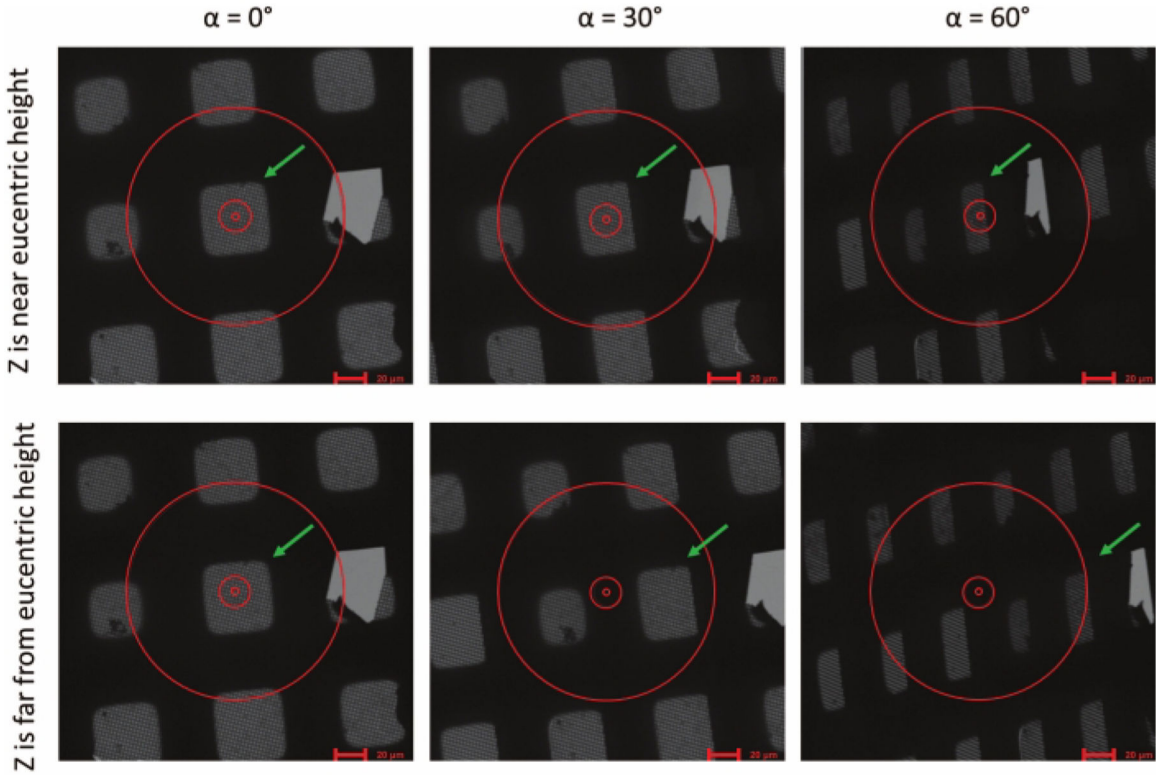

Figure 3: Representative images of the grid at square magnification with different tilt angles. Images collected near and far from eucentric Z-height are shown on the top and bottom panels, respectively. The optical axis of the beam is indicated by the center of the red concentric rings. The green arrow indicates the square of interest. There is a broken grid feature adjacent to the square of interest for reference. The objective aperture is removed for ease of viewing. Scale bar = 20 μM.

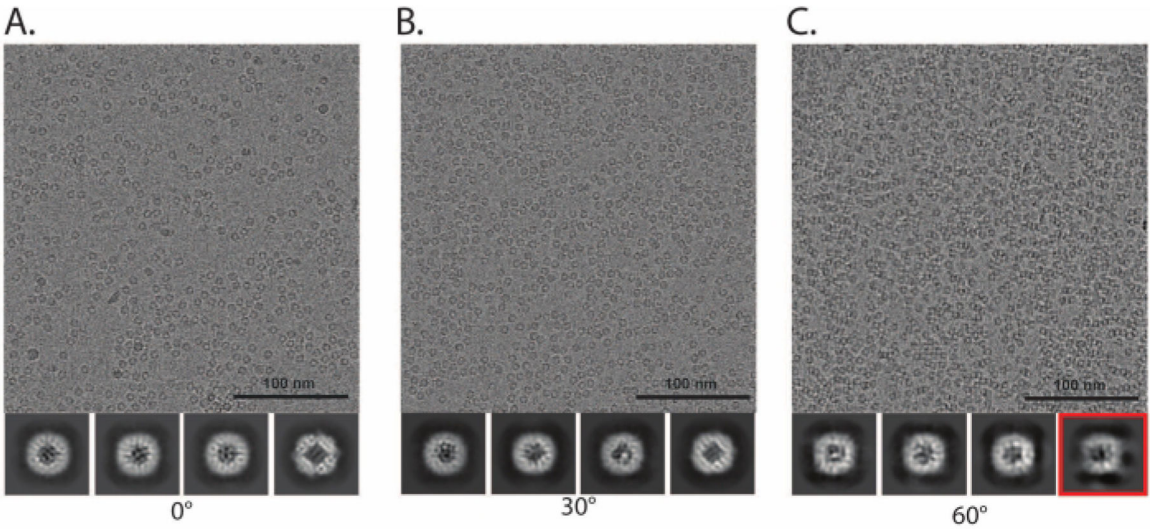

Figure 4: Representative hole exposures and 2D class averages collected at different tilt angles. Panels (**A**), (**B**), and (**C**) refer to imaging performed with the specimen stage untilted at 0° or tilted to 30° and 60°. 2D class averages affected by overcrowding are shown in the red box in (**C**). Scale bar = 100 nm.